
*17th World Conference on Earthquake Engineering, 17WCEE*
*Sendai, Japan - September 13th to 18th 2020*

# DYNAMIC SHEAR FORCES IN COLUMNS OF EARTHQUAKE-RESISTANT REINFORCED CONCRETE FRAMES WITH INTERMEDIATE AND HIGH-STRENGTH REINFORCEMENT

D.V. To[(1)], F. Setiawan[(2)], J.P. Moehle[(3)]

[(1)] *Software Engineer, Computers and Structures, Inc., CA, USA (email: duy@csiamerica.com)*
[(2)] *Structural Designer, Rutherford + Chekene, Inc., CA, USA (email: fsetiawan@ruthchek.com)*
[(3)] *Ed & Diane Professor of Structural Engineering, Dept. of Civil and Environmental Engineering, University of California, Berkeley, CA, USA (email: moehle@berkeley.edu)*

## *Abstract*

Estimation of column shear in seismic design of reinforced concrete special moment resisting frame buildings is challenging because the shear is occurring in columns of a frame in which the columns are designed to remain mainly in the linear range of response with primary yielding in the beams. It has been recognized that current methods for approximating design column shear in special moment frames do not always result in conservative estimates of shear forces that columns need to resist. Underestimation of shear demand in columns could lead to column shear failure, which could cascade to more global response deficiencies, possibly including local or global collapse. Methods for improving the estimation of column shear are investigated through nonlinear dynamic analyses of tall reinforced concrete special moment resisting frames with conventional Nominal Grade 60 (414 MPa) and high-strength reinforcement [Nominal Grade 100 (690 MPa)]. Analytical models of the frame buildings are subjected to ground motions of various categories of earthquake sources including shallow crustal (ordinary and near-fault with velocity pulses) and subduction (interface and slab) tectonic environments.

*Keywords: column shear, special moment frames, high-strength reinforcement, intermediate reinforcement*

 



## 1. Introduction

Column shear failure is relatively brittle and can lead to the rapid loss of shear resistance and axial load-carrying capacity. Shear failure of one or more columns in a story can trigger a story mechanism, which could cascade to more global response deficiencies, possibly including local or global collapse. Column shear failure is one of the most frequently cited sources of reinforced concrete building failure and collapse under earthquake shaking.

Estimating column shear in seismic design is especially challenging. The most reliable approach is to perform nonlinear dynamic analysis under multiple ground motions and determine the column design shears based on statistical evaluation of the results [1]. However, this procedure is computationally expensive and not feasible for preliminary design. ACI 318-19 [2] provides simplified methods and contains requirements for calculation of the column design shear force. Nevertheless, these approaches do not always result in conservative estimates of shear forces that columns need to resist [3, 4, 5, 7].

In this study, nonlinear dynamic analysis is performed for several sets of 10- and 20-story tall reinforced concrete special moment resisting frames with conventional Grade 60 (414 MPa) and high-strength reinforcement [Grade 100 (690 MPa)] subjected to multiple ground motions of various categories of earthquake sources including shallow crustal (ordinary and near-fault with velocity pulses) and subduction (interface and slab) tectonic environments. To assess the design method of ACI 318-19, the column shear forces obtained from dynamic analysis are compared with shear forces calculated according to ACI 318-19 procedures. An alternative approach to obtain improved estimates of the column design shear force is presented.

## 2. Description and Design of Archetype Buildings

Visnjic et al. (2015) [3] considered a set of four 20-story buildings that had identical floor plans and elevations (Fig. 1.) These buildings had two reinforced concrete special moment resisting frames (SMRFs) as seismic-force-resisting systems in each of the two principal directions, located along the perimeter of the floor plan. The frames had four 21-ft (6.4 m) long bays and twenty 12-ft (3.7 m) tall stories to result in building height of 240 ft (73.2 m). The four buildings were designed to have different column sizes and reinforcement ratios. All reinforcement was conventional Grade 60 (414 MPa). The design floor live load was 60 psf (2.87 kN/m$^2$). All buildings were designed according to ASCE 7-10 and ACI 318-11 provisions. These archetype buildings were considered to be at a site in Los Angeles, California.

Recently, several steel mills in the United States can produce reinforcing steel of Grade 100 [nominal yield strength of 100 ksi (690 MPa)]. However, at the time of this writing, none of these higher grades can match the benchmark mechanical properties of Grade 60 A706 steel (414 MPa) (Fig. 2), raising questions about the performance characteristics of reinforced concrete construction that uses the higher-grade reinforcement. The archetype building studied in Visnjic et al. (2015) [3] was re-designed with Grade 60 (414 MPa) and Grade 100 (690 MPa) reinforcement based on design requirements per ASCE 7-16 and ACI 318-14 [7]. Four 20-story building models were obtained, one with conventional Grade 60 A706 (SBH60) reinforcement, one with Grade 100 reinforcement having tensile-to-yield strength ratio (T/Y) of 1.26 (SBH100), one with Grade 100 reinforcement having T/Y = 1.17 (SBL100), and one with Grade 100 A1035 (SBM100) reinforcement. Figure 2 shows the reinforcement stress-strain relationships. The design with conventional Grade 60 reinforcement serves as the base model. From this base design, the dimensions of all structural members are kept the same and all reinforcement is replaced with Grade 100 steel. Thus, the amount of reinforcement in all structural members is reduced appropriately to provide equivalent nominal strengths. By code-based design with linear elastic analysis, the designs of all four archetype frame buildings with normal and higher-grade steel are similar except for the amount of reinforcement. All three buildings with Grade 100 are identical in design. The design floor live load was 60 psf (2.87 kN/m$^2$) and these buildings were hypothetically located in the financial district of downtown San Francisco, California.



 



A third set of building models was also considered. Similar to the buildings described in the preceding paragraph, a set of four 10-story buildings was designed with conventional Grade 60 and high-strength Grade 100 reinforcement. These buildings had the same plan and elevation views as those 20-story buildings in Visnjic et al. (2014) [3] and To (2018) [7], except the number of stories was reduced to ten. All beams and columns were designed to have dimensions of 32 in. height by 20 in. width and 32 in. by 32 in., respectively. For the frame with Grade 60 reinforcement, there were 5 No. 10 bars for top and bottom longitudinal reinforcement in all beams, and 16 No. 10 bars for perimeter longitudinal reinforcement in all columns. All beam and column longitudinal reinforcement was replaced by No. 8 for the other three frames with Grade 100 reinforcement. These 10-story buildings were also hypothetically located in the financial district of downtown San Francisco, California. The design floor live load was 60 psf (2.87 kN/m$^2$).

A fourth set of 10-story archetype buildings was studied by Setiawan (2018) [11]. These buildings had four 24-ft (7.3 m) bays and typical story height was 12 ft (3.7 m), with two reinforced concrete special moment resisting frames as the seismic-force-resisting system in each of the two principal directions on the perimeter of the building. The design used conventional Grade 60 reinforcement and was based on ASCE 7-16 and ACI 318-14. The hypothetical building site was downtown Seattle, Washington.

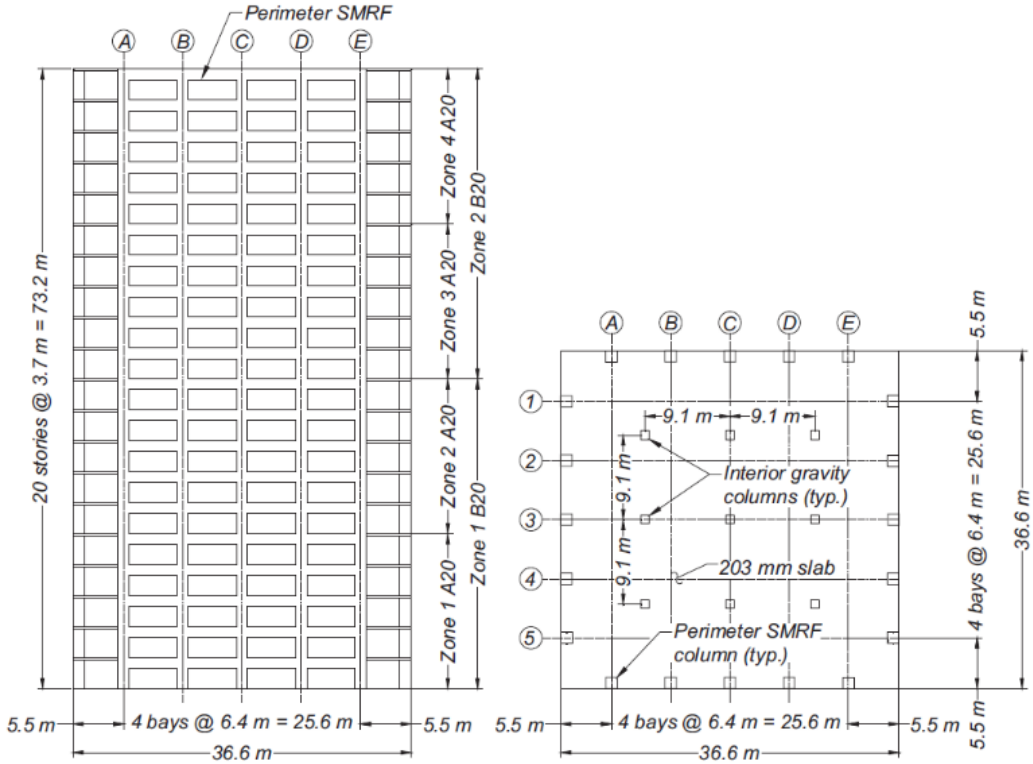


Fig. 1 – Left: Elevation View and Right: Plan View of Archetype Buildings (Visnjic et al. 2014)

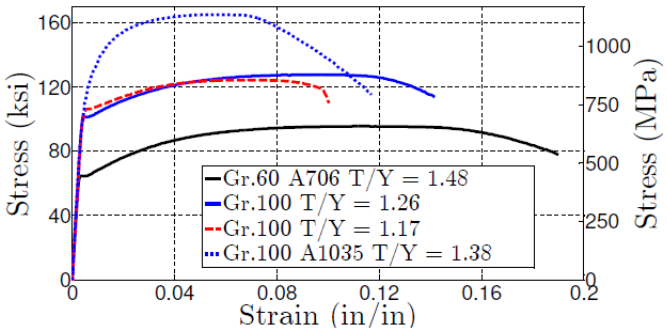


Fig. 2 – Mechanical Properties of Grade 60 and Grade 100 Reinforcing Bars (To et al. 2018)



 



All buildings described in the preceding paragraphs were designed considering load combinations: 1.2$D$ + 1.6$L$, (1.2 + 0.2$S_{DS}$)$D$ + 1.0$E$ + 0.5$L$, and (0.9 – 0.2$S_{DS}$)$D$ + 1.0$E$ where $D$ = dead load, $L$ = live load, $E$ = earthquake load, and $S_{DS}$ = design spectral acceleration parameter at short periods (ASCE 7). The code-prescribed Modal Response Spectrum Analysis (MRSA) procedure was used for seismic design. The square root of sum of square (SRSS) or complete quadratic combination (CQC) was used as the modal combination rule for the first twelve (12) modes in the MRSA, which accounted for more than 98% of the modal mass. The applicable response modification factor was $R = 8$. Column moment strength generally was governed by the ACI 318 requirement that the sum of column nominal moment strengths be at least 6/5 times the sum of beam nominal moment strengths at each beam-column joint. In design, the effective (cracked) stiffnesses used for beams and columns were $0.35E_cI_g$ and $0.5E_cI_g$, respectively, where $I_g$ = gross section moment of inertia and $E_c = 57{,}000\sqrt{f_c'}\ (psi)$ = elastic modulus of concrete.

Tables 1 through 4 summarize the dimensions and reinforcement of the design frames in all studies included in this investigation.

Table 1 – Frame Element Sizes and Steel Ratios (source: Visnjic et al. 2015 [3]) ($b$ = width, $h$ = height, $\rho_l$ = longitudinal reinforcement ratio, $\rho_t$ = transverse reinforcement ratio). Note: * = $\rho_t$ in the first-story column only.

| | | A20-1 | | | | B20-1 | | B20-2 | | B20-3 | |
|---|---|---|---|---|---|---|---|---|---|---|---|
| | Zone | 1 | 2 | 3 | 4 | 1 | 2 | 1 | 2 | 1 | 2 |
| | Stories | 1-5 | 6-10 | 11-15 | 16-20 | 1-10 | 11-20 | 1-10 | 11-20 | 1-10 | 11-20 |
| Beam | $b$ (mm) | 609 | 609 | 609 | 609 | 609 | 609 | 609 | 609 | 609 | 609 |
| | $h$ (mm) | 1067 | 1067 | 914 | 914 | 1067 | 914 | 1067 | 914 | 1067 | 914 |
| | $\rho_l$ (%) | 2.2 | 2.2 | 1.8 | 1.8 | 2.2 | 1.8 | 2.2 | 1.8 | 2.2 | 1.8 |
| | $\rho_t$ (%) | 1.0 | 1.0 | 0.9 | 0.9 | 1.0 | 0.9 | 1.0 | 0.9 | 1.0 | 0.9 |
| Exterior Column | $b$ (mm) | 1219 | 1219 | 1067 | 1067 | 1219 | 1219 | 1524 | 1524 | 1829 | 1829 |
| | $h$ (mm) | 1219 | 1219 | 1067 | 1067 | 1219 | 1219 | 1524 | 1524 | 1829 | 1829 |
| | $\rho_l$ (%) | 2.8 | 1.1 | 1.1 | 1.0 | 2.8 | 2.8 | 2.0 | 2.0 | 1.7 | 1.7 |
| | $\rho_t$ (%) | 2.1* 1.2 | 1.2 | 1.2 | 1.2 | 2.1* 1.2 | 1.2 | 1.9* 1.2 | 1.2 | 1.9* 1.2 | 1.2 |
| Interior & Middle Column | $b$ (mm) | 1219 | 1219 | 1067 | 1067 | 1219 | 1219 | 1219 | 1219 | 1219 | 1219 |
| | $h$ (mm) | 1219 | 1219 | 1067 | 1067 | 1219 | 1219 | 1219 | 1219 | 1219 | 1219 |
| | $\rho_l$ (%) | 1.5 | 1.0 | 1.1 | 1.0 | 1.5 | 1.5 | 1.5 | 1.5 | 1.5 | 1.5 |
| | $\rho_t$ (%) | 1.9* 1.6 | 1.6 | 1.6 | 1.6 | 1.9* 1.6 | 1.6 | 1.9* 1.6 | 1.6 | 1.9* 1.6 | 1.6 |

Table 2: Frame Element Dimensions and Reinforcement of The Third Set of Frame Building Models

| **Design** | | **Grade 60** | **Grade 100** |
|---|---|---|---|
| **Beam** | $b$ (in.) [mm] | 20 [508] | 20 [508] |
| | $h$ (in.) [mm] | 32 [813] | 32 [813] |
| | Top & Bottom Reinforcement | 5 No. 10 | 5 No. 8 |
| | $f_c'\ (psi)$ $[MPa]$ | 5,000 [34.5] | 5,000 [34.5] |
| **Column** | $b$ (in.) [mm] | 32 [813] | 32 [813] |
| | $h$ (in.) [mm] | 32 [813] | 32 [813] |
| | Perimeter Reinforcement | 16 No. 10 | 16 No. 8 |
| | $f_c'\ (psi)$ $[MPa]$ | 6,000 [41.4] | 6,000 [41.4] |



 



Table 3: Frame Element Dimensions and Reinforcement of Design Frames (source: To, 2018 [7])

| **Design** | | **Grade 60** | | | | **Grade 100** | | | |
|---|---|---|---|---|---|---|---|---|---|
| **Zone** | | 1 | 2 | 3 | 4 | 1 | 2 | 3 | 4 |
| **Story** | | 1-5 | 6-10 | 11-15 | 16-20 | 1-5 | 6-10 | 11-15 | 16-20 |
| **Beam** | $b$ (in.) [mm] | 24 [610] | 24 [610] | 24 [610] | 24 [610] | 24 [610] | 24 [610] | 24 [610] | 24 [610] |
| | $h$ (in.) [mm] | 40 [1015] | 40 [1015] | 40 [1015] | 40 [1015] | 40 [1015] | 40 [1015] | 40 [1015] | 40 [1015] |
| | Top & Bottom Reinforcement | 7 No. 10 | 7 No. 10 | 7 No. 9 | 7 No. 9 | 5 No. 9 | 5 No. 9 | 5 No. 8 | 5 No. 8 |
| | $f_c'$ $(psi)$ $[MPa]$ | 5,000 [34.5] | 5,000 [34.5] | 5,000 [34.5] | 5,000 [34.5] | 5,000 [34.5] | 5,000 [34.5] | 5,000 [34.5] | 5,000 [34.5] |
| **Exterior Column** | $b$ (in.) [mm] | 42 [1070] | 42 [1070] | 36 [914] | 36 [914] | 42 [1070] | 42 [1070] | 36 [914] | 36 [914] |
| | $h$ (in.) [mm] | 42 [1070] | 42 [1070] | 36 [914] | 36 [914] | 42 [1070] | 42 [1070] | 36 [914] | 36 [914] |
| | Perimeter Reinforcement | 28 No. 10 | 20 No. 9 | 20 No. 9 | 20 No. 9 | 24 No. 9 | 16 No. 8 | 16 No. 8 | 16 No. 8 |
| | $f_c'$ $(psi)$ $[MPa]$ | 8,000 [55.2] | 8,000 [55.2] | 7,000 [48.3] | 7,000 [48.3] | 8,000 [55.2] | 8,000 [55.2] | 7,000 [48.3] | 7,000 [48.3] |
| **Interior Column** | $b$ (in.) [mm] | 42 [1070] | 42 [1070] | 36 [914] | 36 [914] | 42 [1070] | 42 [1070] | 36 [914] | 36 [914] |
| | $h$ (in.) [mm] | 42 [1070] | 42 [1070] | 36 [914] | 36 [914] | 42 [1070] | 42 [1070] | 36 [914] | 36 [914] |
| | Perimeter Reinforcement | 20 No. 9 | 20 No. 9 | 20 No. 9 | 20 No. 9 | 16 No. 8 | 16 No. 8 | 16 No. 8 | 16 No. 8 |
| | $f_c'$ $(psi)$ $[MPa]$ | 8,000 [55.2] | 8,000 [55.2] | 7,000 [48.3] | 7,000 [48.3] | 8,000 [55.2] | 8,000 [55.2] | 7,000 [48.3] | 7,000 [48.3] |

Table 4: Frame Element Dimensions and Reinforcement of Design Frames (source: Setiawan, 2018 [11])

| | | |
|---|---|---|
| **Beam** | $b$ (in.) [mm] | 18 [457] |
| | $h$ (in.) [mm] | 24 [610] |
| | Top & Bottom Reinforcement | 3 No. 6 |
| | $f_c'$ $(psi)$ $[MPa]$ | 4,000 [27.6] |
| **Column** | $b$ (in.) [mm] | 28 [711] |
| | $h$ (in.) [mm] | 28 [711] |
| | Perimeter Reinforcement | 16 No. 7 |
| | $f_c'$ $(psi)$ $[MPa]$ | 4,000 [27.6] |



 



## 3. Numerical Models

A two-dimensional numerical model of a single special moment frame in each archetype building was constructed and nonlinear history analysis (NRHA) was performed using the Open System for Earthquake Engineering Simulation (OPENSEES) software platform.

Seismic mass was lumped, and gravity load was applied at the joints. All columns at the base level were fixed to the "ground." All beams and columns were modeled using force-based Euler-Bernoulli nonlinear fiber-section frame elements with five Gauss-Lobatto integration points and $P-\Delta$ geometric transformation. Slab effects on beam stiffness and strength were considered in the numerical model of the archetype building in Setiawan (2018) [11] but not considered in the models in Visnjic et al. (2015) [3], To (2018) [7], and the third set of models in this study. Strain penetration of beam longitudinal reinforcement into the beam-column joints and column longitudinal reinforcement into the foundation were modeled through nonlinear rotational springs using zero-length section elements in the models in Visnjic et al. (2015) [3], To (2018) [7], and the third set of building models. Shear behavior in the beams was only modeled by linear elastic property. Strain penetration and shear behavior in the beams were not modeled in the building models studied by Setiawan (2018) [11]. In all frame models of all studies, expected material properties were used.

*Damping forces*: initial stiffness Rayleigh damping, tangent stiffness Rayleigh damping, and modal damping models were implemented in the frame models in Visnjic et al. (2015) [3], To (2018) [7] and the third set of models, and Setiawan (2018) [11], respectively. To (2018) [7] presents a study of the effects of damping models.

## 4. Seismic Hazards and Ground Motions

In Visnjic et al. (2015) [3], a set of fourteen ground motions was selected and linearly scaled such that the mean spectrum approximately matched the smooth design spectra at DBE and $MCE_R$ levels over the period range of interest. This set of motions consisted of fault-normal components of near-fault pulse-like motions that had distinct velocity pulses due to directivity effects.

In To (2018) [7], twenty ground motions were selected such that the average spectrum of fault-normal (FN) component spectra of all ground motions approximates the $MCE_R$ response spectrum. From these selected motions, each fault-parallel (FP) component spectrum was scaled to agree with the RotD50 response spectrum. The set of 20 selected ground motions contains about ten near-fault pulse-like motions that have distinct velocity pulses due to directivity effects. These ground motions were also utilized in the dynamic analysis of the third set of 10-story frame models included in this study.

In Setiawan (2018) [11], a set of twenty ground motions was selected for each seismic source including crustal, crustal with pulses, subduction interface, and subduction slab. They were scaled to the $MCE_R$ uniform hazard spectrum based on agreement with the spectral shape, seismic source, path, and site parameters.

## 5. Analysis Results: Column Shear

According to ACI 318-19, the column design shear force shall be calculated from considering the maximum forces that can be generated at the faces of the joints at each end of the column. These forces shall be calculated using the maximum probable moment strengths, $M_{pr,col}$, at each end of the column associated with the range of factored axial forces, $P_u$, acting on the column, that is, $V_{u,i} = \sum M_{pr,col,i}/l_{u,i}$ (Fig. 3.) In tall buildings with large columns, this approach is known to result in large overestimation of column shears, and the transverse reinforcement required in some cases might be unfeasible to construct. Recognizing this, ACI 318-19 allows that the column shears need not exceed those calculated from joint strengths based on $M_{pr,beam}$ of the beams framing into the joint. A widespread practice is to assume that the probable moment from the beams is resisted by equal column moments above and below the joint, resulting in column shear $V_{u,i} \approx \sum M_{pr,beam,i}/2l_{u,i}$. In the first story of buildings with fixed-base columns, one of the values in $\sum M_{pr,beam,i}$



 



is replaced by $M_{pr,col}$ at base of the building. A drawback of determining shears based on the beam moments is that the distribution of column moments above and below any beam-column joint is indeterminate. Studies (e.g., Kelly 1974 [12]) show that moment patterns can vary widely during seismic response. As a measure to avoid underestimating column design shear force when it is determined from the beam moments, ACI 318-19 also requires that the column design shear force shall be at least the shear from the controlling load combination determined by (linear) analysis of the structure. This latter provision seldom controls the column design.

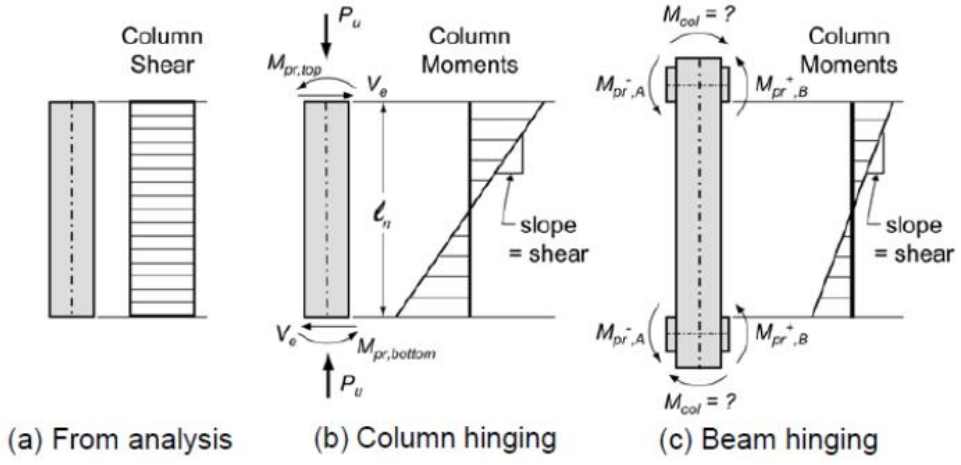


Fig. 3 – Design shear in columns in accordance to ACI 318-19 (source: NIST GCR 8-917-1)

Visnjic et al. (2015) [3], Moehle (2014) [5], and To (2018) [7] proposed that an improved estimate of column design shear force can be obtained by amplifying the shear force obtained from the linear analysis of the structure. The amplification factors consider system overstrength and dynamic effects. Based on this procedure, design column shears can be calculated by:

$$V_u = \omega \Omega_0 V_{MRSA} + V_G \tag{1}$$

where $V_G$ = column shear due to gravity load with combination of $1.0D + 0.25L$
$V_{MRSA}$ = column shear obtained from modal response spectrum analysis
$\omega$ = 1.3 as a dynamic amplification factor
$\Omega_0$ = overstrength of the structural system, which can be approximated as

$$\Omega_0 = \frac{\sum M_{pr}}{\sum M_{u,MRSA}} \tag{2}$$

$\sum M_{pr}$ = sum of probable moment strengths of all beam and column plastic hinges in a beam-yielding mechanism extending the full height of the building. For columns, $M_{pr}$ is estimated assuming axial load corresponding to gravity load of $1.0D + 0.25L$.

$\sum M_{u,MRSA}$ = sum of the moments calculated from modal response spectrum analysis at all beam and column plastic hinge locations of the same beam-yielding mechanism in absence of gravity loads.

Note that column shear in Eq. (1) could also include effects of vertical seismic actions using load combinations of ASCE 7. However, such effects were not represented in the dynamic analyses presented here, so they are not included in the design equation either.

Column shear forces calculated by these various approaches are plotted and compared against the average of the column shears from nonlinear dynamic analyses in Fig. 4-7. The shear is normalized by $A_g\sqrt{f_c'}$ where $A_g$ is in $m^2$ and $f_c'$ is in $MPa$. As expected, $V_{u,i} = \sum M_{pr,col,i}/l_{u,i}$ (presented as ACI 318 Method A in Fig. 4 by Visnjic et al. 2015 [3]) results in large overestimation of column shears in all cases. $V_{u,i} = \sum M_{pr,beam,i}/2l_{u,i}$ (shown as ACI 318 Method B2 in Fig. 4 [3]) provides a reasonable central approximation of the shears, but underestimation or overestimation in individual stories appears to be unacceptably large. The



 



shear obtained from the controlling load combination determined by linear analysis of the structure $V_{MRSA}$ is well below the shear obtained from nonlinear dynamic analysis, as is typically the case. The last approach of amplifying $V_{MRSA}$ in accordance with Eq. (1) produces the best overall estimate of shear in all exterior, interior, and middle columns. However, it is worth noting that shear in the exterior columns of the first story is underestimated by this method as it does not account for the effects of beam elongation, which pushes the first-story columns outward, thereby increasing the first-story shear [3, 5, 7].

It can also be observed that the method presented by Eq. (1) slightly overestimates shear in exterior columns for frames SBH100 and SBL100 as these frames are reinforced with higher-grade steel that has lower strain-hardening ratio than that of conventional Grade 60 A706. Hence, the overstrength factor of the structural system is overestimated for these two frames.

Overall, it appears that shear calculated by Eq. (1) modestly overestimates shear in interior and middle columns in the lower stories of all frame models. On the other hand, it slightly underestimates shear in all columns in the upper stories of all buildings, possibly due to the dynamic effects of higher modes of response on the shear distribution in multistory reinforced concrete frame [3, 4, 7, 11, 13, 14].

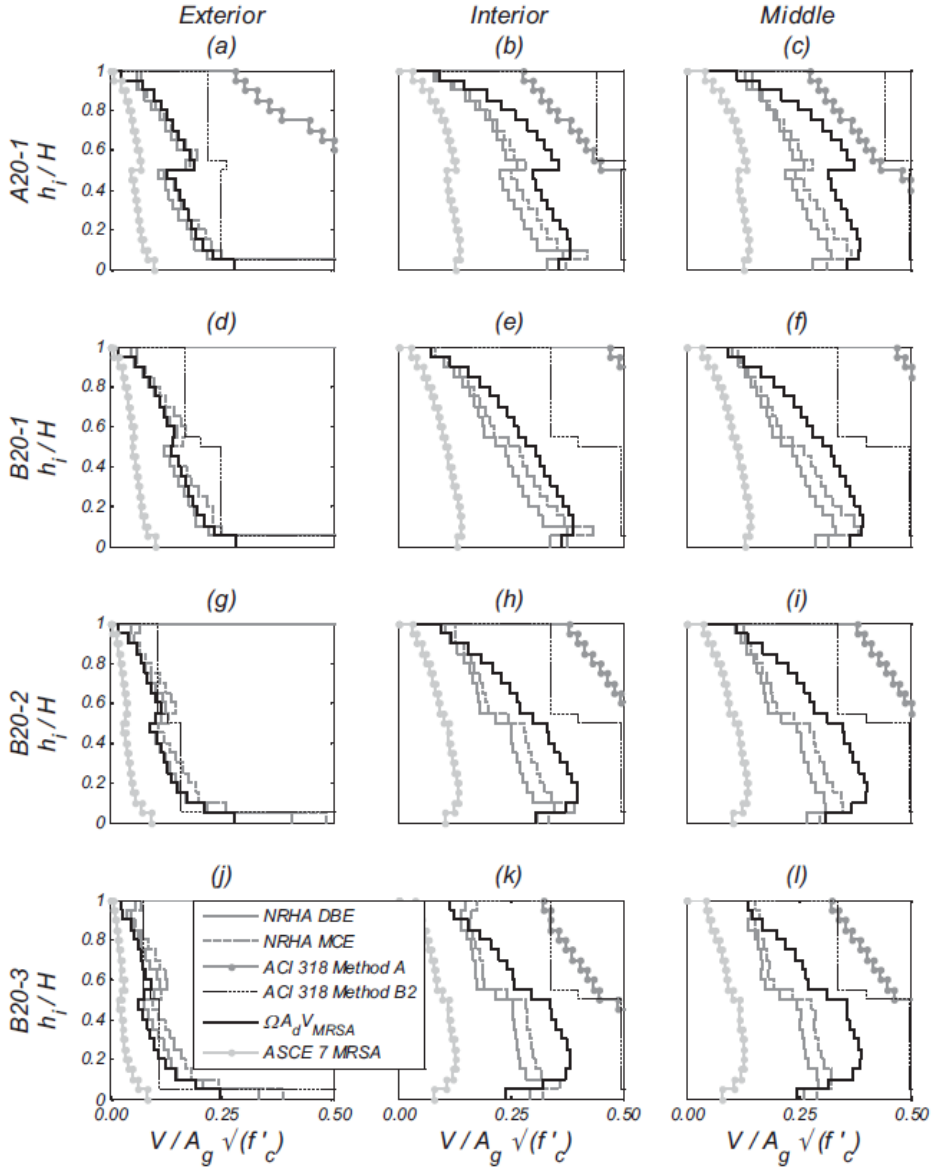


Fig. 4 – Column shear response comparison (source: Visnjic et al. 2015)



 



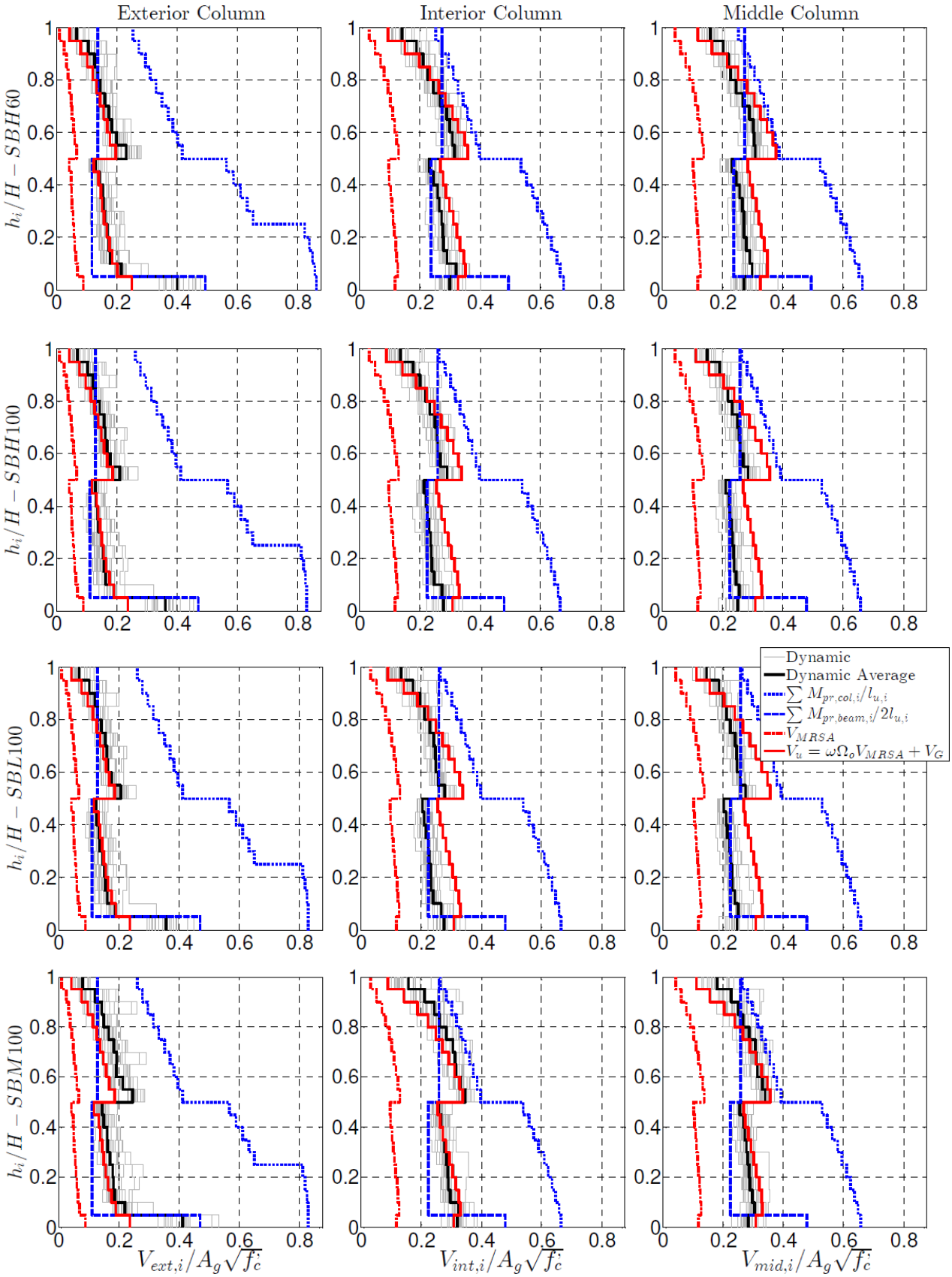


Fig. 5 – Column shear response comparison (source: To, 2018 [7])



 



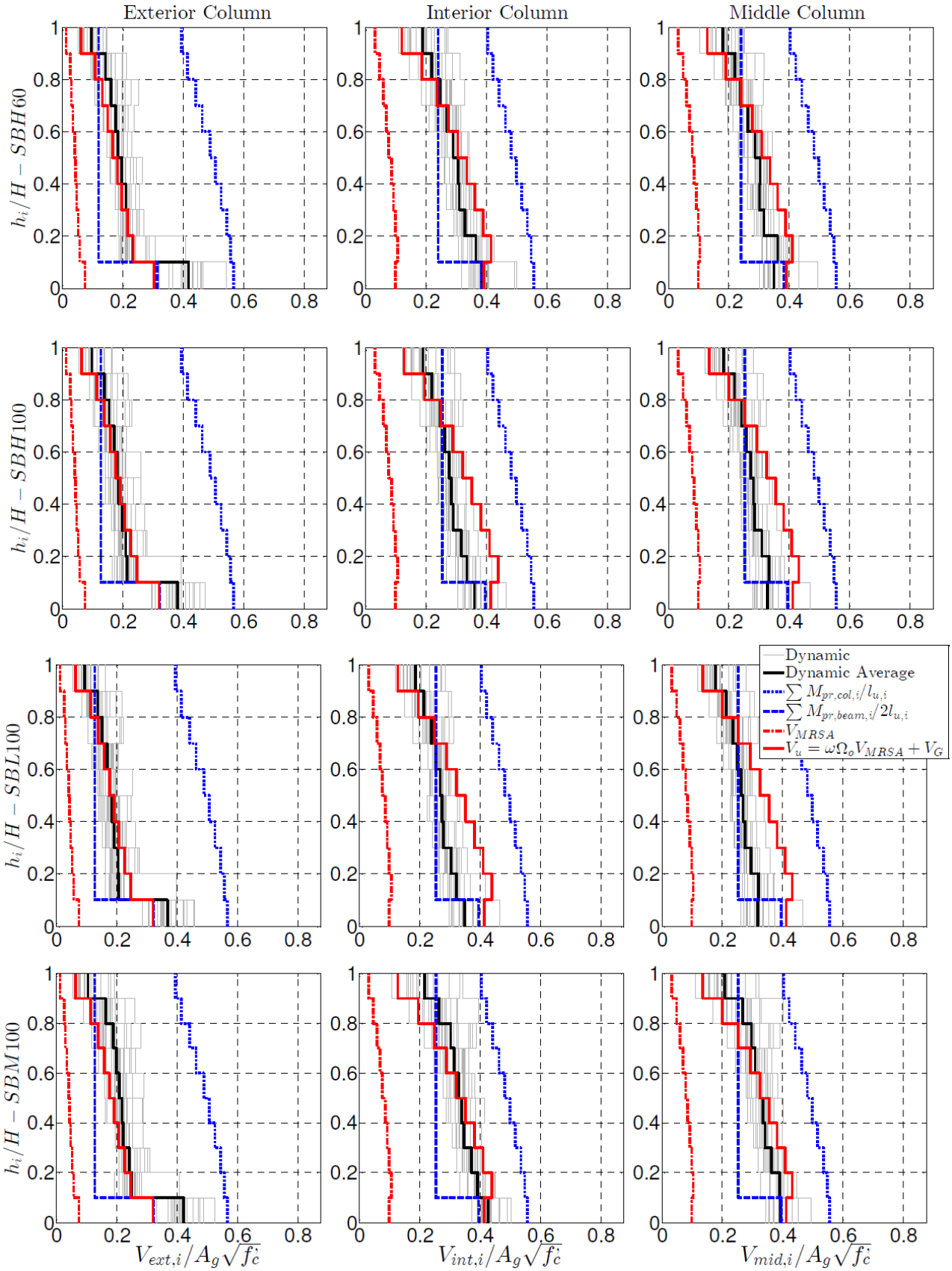


Fig. 6 – Column shear response comparison – 10-story buildings with high-strength reinforcement



 



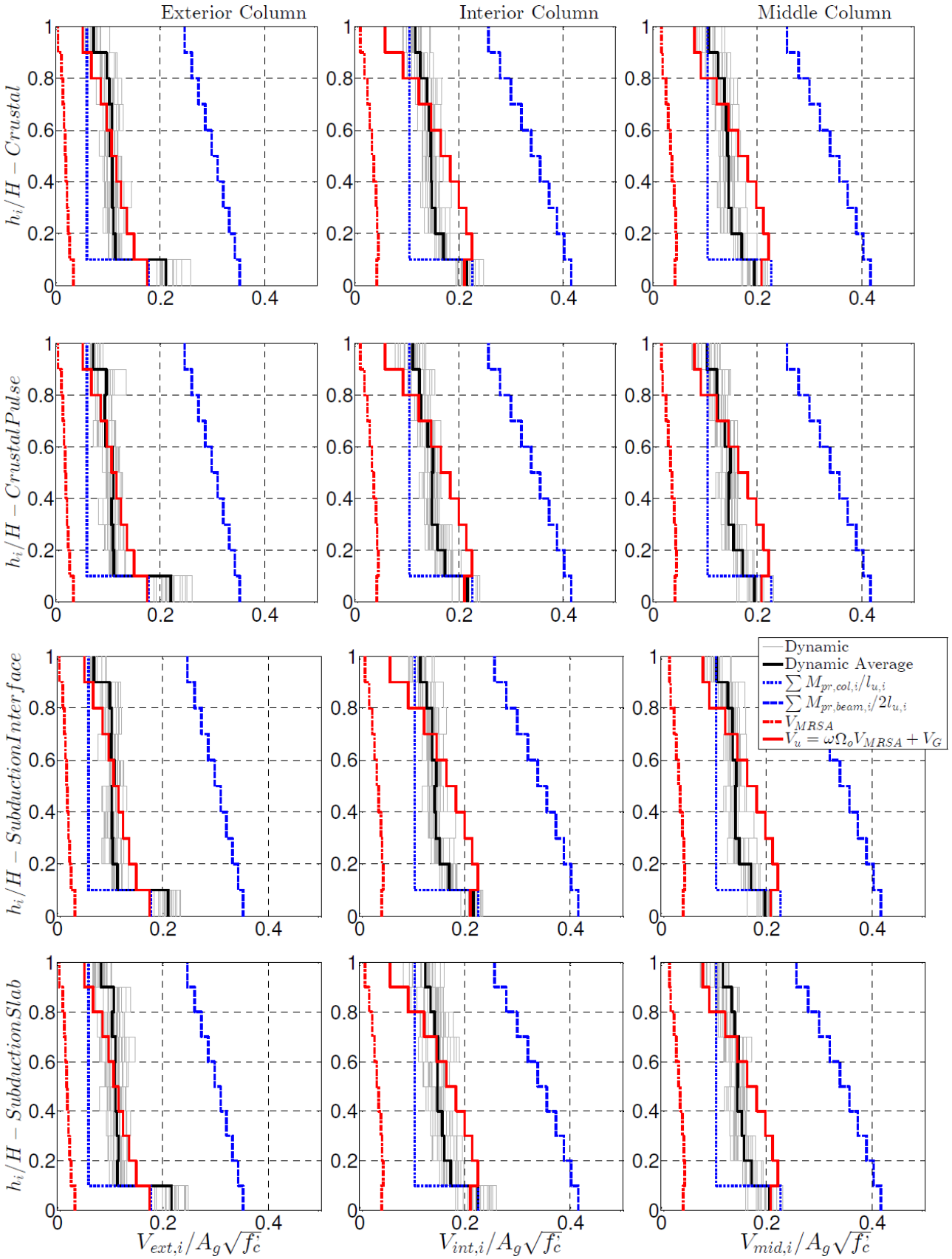


Fig. 7 – Column shear response comparison (source: Setiawan, 2018 [11])



 



## 6. Conclusions

ACI 318-19 procedures for determining the column design shear forces can significantly underestimate shears calculated by nonlinear dynamic analysis. An alternative approach is presented that produces improved estimates of design shears. The proposed method is based on the shears calculated from elastic, code-prescribed modal response spectrum analysis results amplified for dynamic and overstrength effects.

## 7. Acknowledgements

The authors would like to thank Computers and Structures, Inc. for providing the software used in design and analysis of the building models in this study.

## 8. References

[1] TBI (2017). *Guidelines for Performance-Based Seismic Design of Tall Buildings*, Report No. 2017/06, Pacific Earthquake Engineering Research Center, University of California, Berkeley, CA, 147 pp.

[2] ACI 318 (2019). *Building Code Requirements for Structural Concrete (ACI 318-19) and Commentary*, American Concrete Institute, Farmington Hills, MI.

[3] Visnjic, T., M. Panagiotou, and J.P. Moehle (2015). "Seismic Response of 20-Story Tall Reinforced Concrete Special Moment Resisting Frames Designed with Current Code Provisions," *Earthquake Spectra*, V. 31, No. 2, pp. 869-893.

[4] Visnjic, T. (2014). *Design Considerations for Earthquake-Resistant Reinforced Concrete Special Moment Frames*, Doctoral Dissertation, University of California, Berkeley, CA.

[5] Moehle, J. P. (2014). *Seismic Design of Reinforced Concrete Buildings*, Mc Graw-Hill Education, New York, 760 pp.

[6] Moehle, J.P., and J.D. Hooper (2016). *Seismic Design of Reinforced Concrete Special Moment Frames: A Guide for Practicing Engineers, Second Edition*, NEHRP Seismic Design Technical Brief No. 1, NIST GCR 16-917-40, National Institute of Standards and Technology, Gaithersburg, MD.

[7] To, D.V. (2018). *Seismic Performance Characterization of Beams with High-Strength Reinforcement*, Doctoral Dissertation, University of California, Berkeley, CA.

[8] ASCE 7 (2010). *Minimum Design Loads for Buildings and Other Structures*, American Society of Civil Engineers, Reston, VA.

[9] ASCE 7 (2016). *Minimum Design Loads for Buildings and Other Structures*, American Society of Civil Engineers, Reston, VA.

[10] ACI 318 (2014). *Building Code Requirements for Structural Concrete (ACI 318-14) and Commentary*, American Concrete Institute, Farmington Hills, MI.

[11] Setiawan F. (2018). *Seismic Performance of Reinforce Concrete Special Moment resisting Frames in Subduction and Shallow Crustal Tectonic Environment*. Master Thesis, University of California, Berkeley, CA.

[12] Kelly, T. (1974). *Some Seismic Design Aspects of Multistorey Concrete Frames*, Master of Engineering Report, University of Canterbury, Christchurch, New Zealand, 163 pp.

[13] Pettinga, J.D. and M.J.N. Priestley (2015). "Dynamic Behaviour of Reinforced Concrete Frames Designed with Direct Displacement-Based Design," *Journal of Earthquake Engineering*, 9(sup. 2): 309-330.

[14] New Zealand Standard NZS3101, 2009. *Concrete Structures Standard, Part 1 – The Design of Concrete Structures*, Wellington, New Zealand.



 